CHEMISTRY OF MATERIALS
Article

Chem. Mater. **2010,** *22,* 5093–5104 5093
DOI:10.1021/cm1017344

Facile Synthesis of Monodisperse Spherical MCM-48 Mesoporous Silica Nanoparticles with Controlled Particle Size

Tae-Wan Kim,*[,‡] Po-Wen Chung,[†] and Victor S.-Y. Lin[†,§]

[†]*Department of Chemistry, U.S. Department of Energy Ames Laboratory, Iowa State University, Ames, Iowa 50011-3111, and* [‡]*Green Chemistry Research Division, Korea Research Institute of Chemical Technology, P.O. Box 107, Sinseongro 19, Yuseong-gu, Daejeon 305-600, Korea.* [§]*Deceased on May 4, 2010. We dedicate this work to his memory*

Received June 22, 2010. Revised Manuscript Received July 14, 2010

A rapid and facile synthesis route to the monodisperse spherical MCM-48 mesoporous silica nanoparticles (MSN) with cubic $Ia\bar{3}d$ mesostructure is developed based on the modified Stöber method. The phase domain of MCM-48-type MSNs can be extended by controlling the stirring rate and molar ratios of silica source and surfactant. The formation of monodispersed spherical MCM-48-type MSNs is obtained using triblock copolymer Pluronic F127 as a particle size designer. The average size of monodisperse spherical MSN can be controlled within the range of 70−500 nm depending on the amount of F127. Moreover, the pore diameter of MSNs can be precisely controllable in pore diameters from 2.3 to 3.3 nm using different alkyl chain surfactants and simple posthydrothermal treatment. An investigation of MCM-48-type MSN materials using powder X-ray diffraction, transmission electron microscopy, scanning electron microscopy, and nitrogen physisorption clearly reveals that MSNs show high specific surface area, high pore volumes, controllable morphological aspects, and tunable pore diameters. The MCM-48-type MSNs thus obtained are demonstrated as a good hard template for the preparation of other mesoporous nanoparticles, such as mesoporous metal oxides. The present discovery of the extended synthesis conditions and the binary surfactant system in MCM-48 synthesis offers reproducible and facile synthesis of the monodisperse spherical MCM-48 mesoporous silica nanoparticles with precise structural control, and thus has vast prospects for future applications of ultrafine mesostructured nanoparticle materials.

1. Introduction

Since the discovery of the M41S family of mesoporous molecular sieves in the early 1990s,[1,2] the field of ordered mesoporous materials using organic−inorganic self-assembly has been considerably studied with regard to mesostructural diversity, compositional flexibility, and control of the pore size and morphology.[3−9] In these studies, the synthesis of monodisperse mesoporous nanoparticles with controllable particle size should be critical because of the many potential applications of chromatography, cosmetics, catalyst, and adsorption,[3,5,6,9−12] as mesoporous nanoparticles provide greater pore accessibility and smooth molecular diffusion. Specially, ultrafine mesoporous nanoparticles below submicrometer size (normally, below 500 nm) could be used in biomedical and pharmaceutical applications such as drug, gene, protein, imaging agents delivery, and biosensors.[8,12−17]

To date, there have been great efforts made in the development of recipes for the preparation of monodisperse mesoporous nanoparticles. The factors for control morphology and particle size of mesoporous nanoparticles are complex and connected to surface energy and cooperative organization between the organic templates

*Corresponding author. E-mail: twkim@krict.re.kr. Phone: +82-42-860-7257. Fax: +82-42-860-7508.

(1) Kresge, C. T.; Leonowicz, M. E.; Roth, W. J.; Vartuli, J. C.; Beck, J. S. *Nature* **1992**, *359*, 710.
(2) Beck, J. S.; Vartuli, J. C.; Roth, W. J.; Leonowicz, M. E.; Kresge, C. T.; Schmitt, K. D.; Chu, C. T. W.; Olson, D. H.; Sheppard, E. W.; McCullen, S. B.; Higgins, J. B.; Schlenker, J. L. *J. Am. Chem. Soc.* **1992**, *114*, 10834.
(3) Corma, A. *Chem. Rev.* **1997**, *97*, 2373.
(4) Zhao, D.; Feng, J.; Huo, Q.; Melosh, N.; Fredrickson, G. H.; Chmelka, B. F.; Stucky, G. D. *Science* **1998**, *279*, 548.
(5) Stein, A. *Adv. Mater.* **2003**, *15*, 763.
(6) Hoffmann, F.; Cornelius, M.; Morell, J.; Fröba, M. *Angew. Chem., Int. Ed.* **2006**, *45*, 3216.
(7) Wan, Y.; Zhao, D. Y. *Chem. Rev.* **2007**, *107*, 2821.
(8) Trewyn, B. G.; Giri, S.; Slowing, I. I.; Lin, V. S. Y. *Chem. Commun.* **2007**, 3236.
(9) Giraldo, L. F.; López, B. L.; Pérez, L.; Urrego, S.; Sierra, L.; Mesa, M. *Macromol. Symp.* **2007**, *258*, 129.
(10) Hartmann, M. *Chem. Mater.* **2005**, *17*, 4577.
(11) Sun, J.; Zhang, H.; Tian, R.; Ma, D.; Bao, X.; Su, D. S.; Zou, H. *Chem. Commun.* **2006**, 1322.
(12) Angelos, S.; Liong, M.; Choi, E.; Zink, J. I. *Chem. Eng. J.* **2008**, *137*, 4.
(13) Radu, D. R.; Lai, C. Y.; Jeftinija, K.; Rowe, E. W.; Jeftinija, S.; Lin, V. S. Y. *J. Am. Chem. Soc.* **2004**, *126*, 13216.
(14) Trewyn, B. G.; Whitman, C. M.; Lin, V. S. Y. *Nano Lett.* **2004**, *4*, 2139.
(15) Slowing, I.; Trewyn, B. G.; Lin, V. S.-Y. *J. Am. Chem. Soc.* **2006**, *128*, 14792.
(16) Vallet-Regí, M.; Balas, F.; Arcos, D. *Angew. Chem., Int. Ed.* **2007**, *46*, 7548.
(17) Torney, F.; Trewyn, B. G.; Lin, V. S. Y.; Wang, K. *Nat. Nanotechnol.* **2007**, *2*, 295.

Published on Web 08/03/2010

and inorganic source components.[18] Thus, monodisperse mesoporous nanoparticles with particle sizes ranging hundreds of nanometers to a few micrometers have been prepared via sol−gel process using various synthetic approaches, which involve extremely diluted reaction solutions, quenching procedures, complexing strategies, spray-drying, emulsion confinement, ionic liquid templating, dry-gel conversion, and binary surfactant system.[5,11,14,19−37] Among these mesoporous silica nanoparticles (MSNs), monodisperse spherical MCM-41-type MSN materials with 2-dimensional (2-D) hexagonal *p6mm* structure using cationic surfactant as a structural directing agent were demonstrated as good intracellular carriers for biomedical and pharmaceutical applications.[8,12−17]

Compared to 2D hexagonal MCM-41 in the M41S family, MCM-48 mesoporous silicas with a three-dimensional (3D) cubic $Ia\bar{3}d$ mesostructure have an interesting mesostructure, which consists of two interpenetrating continuous networks of chiral channels.[1,2,38,39] These enantiomeric pairs of porous channels are separated by an inorganic wall that follows exactly the gyroid (*G*-surface) infinite periodic minimal surface (IPMS).[40,41] This unique 3D channel network is thought to provide a highly opened porous host that provides easy and direct access for guest species, thus facilitating inclusion or diffusion throughout the pore channels without pore blockage.[38] Although these properties attract increasing attention in terms of their potential use as catalyst, adsorbent, host for nanostructures and "hard template" for the fabrication of nano-objects,[3,9,10,42−45] the synthesis of monodisperse spherical MCM-48-type MSN materials with cubic $Ia\bar{3}d$ mesophase still remains challenging. Conventionally, the synthesis of MCM-48 materials is carried out through hydrothermal routes, but the hydrothermal synthesis methods typically take a long time, require high temperatures, and have a narrow range of compositions.[2,38,46] Moreover, it gives a large particle size above 1 μm with irregular morphologies. In contrast to the hydrothermal recipes, the modified Stöber method proposed by Schumacher et al. requires only a short synthesis time at room temperature.[47,48] This recipe produces spherical MCM-48 mesoporous silica nanoparticles below 1 μm, but it is not fully monodispersed and the individual silica particle is still large for the intracellular bioapplications, which is the same as MCM-41-type MSNs. Very recently, new synthesis pathways utilizing a laboratory designed glycol-modified silanes, as the silica source been proposed for the generation of the MCM-48-type cubic sphere.[49]

In the present work, we discovered that monodisperse spherical MCM-48-type mesoporous silica nanoparticles could be synthesized under the conditions of low surfactant/silicon ratio with high stirring rate based on a modified Stöber method. The phase domain for the cubic $Ia\bar{3}d$ mesophase could be extended, while the amounts of silica source and surfactant were changed correspondingly. Monodisperse spherical MCM-48 nanoparticles with controllable particle size were obtained by using Pluronic F127 as a dispersing agent, and the pore size can be tuned using different alkyl chain length of surfactant and simple posthydrothermal treatment. In addition, we demonstrated the synthesis of a series of mesoporous metal oxide nanoparticles by using the MCM-48-type MSNs as a hard template.

2. Experimental Section

2.1. Preparation of MCM-48 MSN. As previously reported, the preparation of MCM-48 ordered mesoporous silica nanoparticles was based on the modified Stöber method.[47,48] The MCM-48-type MSNs were synthesized under various synthetic conditions using a mixture of cetyltetramethylammonum bromide (CTAB, Aldrich) and ethanol as a structure-directing mixture. Tetraethyl orthosilicate (TEOS, Gelest Inc.) and triblock copolymer F127 (Pluronic F127, $EO_{106}PO_{70}EO_{106}$) were applied as a silica source and a particle dispersion agent, respectively.[29,31] The molar composition of the reaction mixture

(18) Cho, E. B.; Kim, D.; Jaroniec, M. *J. Phys. Chem. C* **2008**, *112*, 4897.
(19) Lu, Y.; Fan, H.; Stump, A.; Ward, T. L.; Rieker, T.; Brinker, C. J. *Nature* **1999**, *398*, 223.
(20) Grun, M.; Lauer, I.; Unger, K. K. *Adv. Mater.* **1997**, *9*, 254.
(21) Cai, Q.; Luo, Z. S.; Pang, W. Q.; Fan, Y. W.; Chen, X. H.; Cui, F. Z. *Chem. Mater.* **2001**, *13*, 258.
(22) Fowler, C. E.; Khushalani, D.; Lebeau, B.; Mann, S. *Adv. Mater.* **2001**, *13*, 649.
(23) Sajanikumari, S.; Fowler, C. E.; Khushalani, D.; Mann, S. *Angew. Chem., Int. Ed.* **2002**, *41*, 2151.
(24) Nooney, R. I.; Thirunavukkarasu, D.; Chen, Y.; Josephs, R.; Ostafin, A. E. *Chem. Mater.* **2002**, *14*, 4721.
(25) Haskouri, J. E.; Zarate, D. O. d.; Guillem, C.; Latorre, J.; Caldes, M.; Beltran, A.; Beltran, D.; Descalzo, A. B.; Rodriguez-Lopez, G.; Martinez-Manez, R.; Marcos, M. D.; Amoros, P. *Chem. Commun.* **2002**, 330.
(26) Zhao, W.; Li, Q. *Chem. Mater.* **2003**, *15*, 4160.
(27) Areva, S.; Boissiere, C.; Grosso, D.; Asakawa, T.; Sanchez, C.; Linden, M. *Chem. Commun.* **2004**, 1630.
(28) Zhang, H.; Sun, J.; Ma, D.; Bao, X.; Klein-Hoffmann, A.; Weinberg, G.; Su, D.; Schlogl, R. *J. Am. Chem. Soc.* **2004**, *126*, 7440.
(29) Suzuki, K.; Ikari, K.; Imai, H. *J. Am. Chem. Soc.* **2004**, *126*, 462.
(30) Han, Y.; Ying, J. Y. *Angew. Chem., Int. Ed.* **2005**, *44*, 288.
(31) Ikari, K.; Suzuki, K.; Imai, H. *Langmuir* **2006**, *22*, 802.
(32) de Zárate, D. O.; Gómez-Moratalla, A.; Guillem, C.; Beltrán, A.; Latorre, J.; Beltrán, D.; Amorós, P. *Eur. J. Inorg. Chem.* **2006**, *2006*, 2572.
(33) Zhang, H.; Sun, J.; Ma, D.; Weinberg, G.; Su, D. S.; Bao, X. *J. Phys. Chem. B* **2006**, *110*, 25908.
(34) Yamada, Y.; Yano, K. *Microporous Mesoporous Mater.* **2006**, *93*, 190.
(35) Shen, S.; Chen, F.; Chow, P. S.; Phanapavudhikul, P.; Zhu, K.; Tan, R. B. H. *Microporous Mesoporous Mater.* **2006**, *92*, 300.
(36) Garcia-Bennett, A. E.; Lund, K.; Terasaki, O. *Angew. Chem., Int. Ed.* **2006**, *45*, 2434.
(37) Zhai, S.-R.; Ha, C.-S. *Microporous Mesoporous Mater.* **2007**, *102*, 212.
(38) Monnier, A.; Schuth, F.; Huo, Q.; Kumar, D.; Margolese, D.; Maxwell, R. S.; Stucky, G. D.; Krishnamurty, M.; Petroff, P.; Firouzi, A.; Janicke, M.; Chmelka, B. F. *Science* **1993**, *261*, 1299.
(39) Kim, T.-W.; Kleitz, F.; Paul, B.; Ryoo, R. *J. Am. Chem. Soc.* **2005**, *127*, 7601.
(40) Carlsson, A.; Kaneda, M.; Sakamoto, Y.; Terasaki, O.; Ryoo, R.; Joo, S. H. *J Electron Microsc* **1999**, *48*, 795.
(41) Alfredsson, V.; Anderson, M. W. *Chem. Mater.* **1996**, *8*, 1141.
(42) Ryoo, R.; Joo, S. H. *Stud. Surf. Sci. Catal.* **2004**, *148*, 241.
(43) Kim, T.-W.; Solovyov, L. A. *J. Mater. Chem.* **2006**, *16*, 1445.
(44) Lee, J.; Kim, J.; Hyeon, T. *Adv. Mater.* **2006**, *18*, 2073.
(45) Bronkema, J. L.; Bell, A. T. *J. Phys. Chem. C* **2007**, *111*, 420.
(46) Vartuli, J. C.; Schmitt, K. D.; Kresge, C. T.; Roth, W. J.; Leonowicz, M. E.; McCullen, S. B.; Hellring, S. D.; Beck, J. S.; Schlenker, J. L.; Olson, D. H.; Sheppard, E. W. *Chem. Mater.* **1994**, *6*, 2317.
(47) Schumacher, K.; Gr, M.; Unger, K. K. *Microporous Mesoporous Mater.* **1999**, *27*, 201.
(48) Schumacher, K.; Ravikovitch, P. I.; Du Chesne, A.; Neimark, A. V.; Unger, K. K. *Langmuir* **2000**, *16*, 4648.
(49) Nakamura, T.; Yamada, H.; Yamada, Y.; Gürtanyel, A.; Hartmann, S.; Hüsing, N.; Yano, K. *Langmuir* **2009**, *26*, 2002.

was varied in the range of x:0.4:12.5y:54y:417y:z TEOS:CTAB:NH_3:EtOH:H_2O:F127 with $x = 1-4.25$, $y = 1-9$, and $z = 0-0.094$. The reaction temperature was fixed at room temperature, and further posthydrothermal treatments were carried out at 403 and 423 K.[50] A typical preparation of MCM-48-type MSN is as follows: 0.5 g of CTAB and 2.05 g of F127 are dissolved in 96 mL of distilled water, 34 g of EtOH, and 10.05 g of 29 wt % ammonium hydroxide solution at room temperature. After complete dissolution, 1.8 g of TEOS is added into the mixture at once. After 1 min of mechanical stirring at 1000 rpm, the mixture was kept at a static condition for 24 h at RT for further silica condensation. The white solid product is recovered by ultrahigh speed centrifuge (Sorvall Evolution Centrifuge), washed with water, and dried at 343 K in air. The final template-free MCM-48 MSN materials are obtained after calcinations at 823 K in air. For the posthydrothermal treatment, the centrifuged sample is placed in the Teflon-lined autoclave with 8.5 mL of distilled water. The hydrothermal temperature varied from 403 to 423 K for 2 days in static conditions.

For pore size control using different alkyl chain lengths of surfactant, the same synthesis described above can be carried out using octadecyltrimethylammonium bromide (OTAB, Aldrich) rather than CTAB. The molar composition of the reaction mixture was varied in the range of 1.75:50:216:0.4:1668:x TEOS:NH_3:EtOH:OTAB:H_2O:F127 with $x = 0-0.047$.

2.2. Preparation of metal oxide nanoparticles. A series of mesoporous metal oxide nanoparticles, iron oxide (Fe_2O_3), cobalt oxide (Co_3O_4), cerium oxide (CeO_2), and indium oxide (In_2O_3), were prepared using MCM-48-type MSN with posthydrothermal treatment at 423 K as a hard template. Metal oxides synthesis was carried out through a repeated impregnation-calcination process.[51,52] For example, the detailed synthesis of mesoporous iron oxide nanoparticles is as follows: 0.15 g of calcined MCM-48 MSN is impregnated with 0.33 g of iron(III) nitrate nonahydrate ($Fe(NO_3)_2 \cdot 9H_2O$, Aldrich) in 0.33 mL of acetone. After drying at 333 K for 2 h, the impregnated sample is calcined at 623 K for 5 h. The sample was added with 0.28 g of $Fe(NO_3)_2 \cdot 9H_2O$ in 0.28 mL of acetone, and heated again. The final impregnation was performed with 0.23 g of iron nitrate in 0.23 mL of acetone, and was heated up to 823 K for 5 h. The template MSN is removed by 1 M NaOH aqueous solution.

2.3. Measurements. Powder XRD patterns were recorded on a Scintag XDS-2000 instrument operated at 1.21 kW, using Cu Kα radiation. The nitrogen adsorption isotherms were measured at liquid nitrogen temperature (77 K) using a Micromeritics ASAP2000 volumetric adsorption analyzer. The Brunauer−Emmett−Teller (BET) equation was used to calculate the apparent surface area from adsorption data obtained at P/P_0 between 0.05 and 0.2. The total volume of micropores and mesopores was calculated from the amount of nitrogen adsorbed at $P/P_0 = 0.95$, assuming that adsorption on the external surface was negligible compared to the adsorption in pores. The pore size distributions (PSD) were calculated by analyzing the adsorption branch of the N_2 sorption isotherm using the Barret−Joyner−Halenda (BJH) method. Scanning electron micrograph (SEM) images were obtained with a JEOL 840A scanning electron microscope operating at 10 kV. The samples were coated with gold before SEM measurement. Transmission electron micrograph (TEM) images were taken from particles supported on a porous carbon grid, using a Tecnai G2 F20 operated at 200 kV.

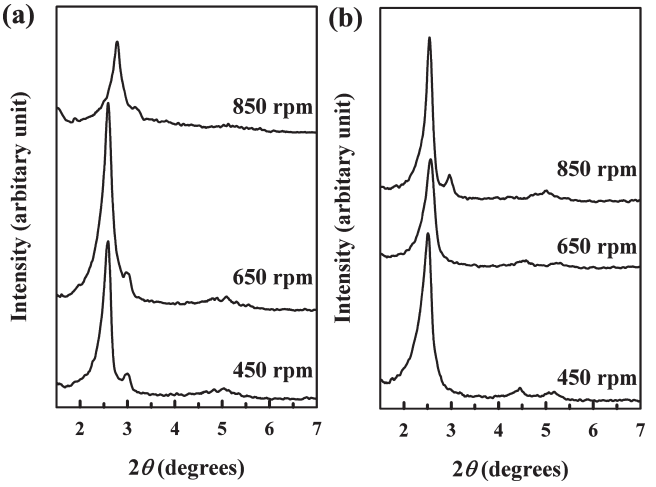

Figure 1. Powder XRD patterns for the calcined mesoporous silica materials obtained using magnetic stirrer with different stirring rate for 4 h, and x:12.5y:54y:0.4:417y TEOS:NH_3:EtOH:CTAB:H_2O. The molar ratios of TEOS (x) and diluted times (y) were (x, y) = (a) (1.0, 1) and (b) (2.5, 4).

3. Results and Discussion

3.1. Effect of CTAB Concentration, and Stirring Rate and Time. Figure 1 shows the powder XRD patterns of template-free mesoporous silica materials obtained at different amounts of TEOS and CTAB, and at different stirring rates. This demonstrates the crucial role of the surfactant/silicon ratio and the stirring rate on the formation of a specific mesophase structure. The silica materials presented were synthesized using the a digital magnetic stirrer (Corning Co.) for 4 h at room temperature with a varying stirring rate. From the powder XRD patterns in Figure 1a, it is clearly evident that the 3D cubic $Ia\bar{3}d$ mesophase is formed at the stirring rate between 450 to 850 rpm with the original modified Stöber method, (TEOS, diluted times) = (1.0, 1). Stirring rates in the range of 450−650 rpm lead to the formation of highly ordered cubic $Ia\bar{3}d$ structures. At 850 rpm, the d-spacings and peak shapes of XRD (211) and (220) reflections are decreased and broaden, which reflects the formation of a low-quality cubic mesostructure. This quality control of MCM-48 synthesis at room temperature can be tuned by stirring rate, which is the similar to the results recently reported by Boote et al.[53] The morphology of these mesostructured MCM-48 silica materials with different stirring rates is nearly spherical but fused together. The particle size of each single spherical particle is varied in the range of 150−600 nm (see Figure S1 in the Supporting Information) In Figure 1b, the 4 times dilution of CTAB with lower silicon ratio, CTAB/TEOS = 0.16, affords 2D hexagonal MCM-41-type mesoporous silica materials at a low stirring rate below 650 rpm. However, the synthesis at the high stirring rate of 850 rpm results in highly

(50) Sun, J.-H.; Coppens, M.-O. *J. Mater. Chem.* **2002**, *12*, 3016.
(51) Tian, B.; Liu, X.; Solovyov, L. A.; Liu, Z.; Yang, H.; Zhang, Z.; Xie, S.; Zhang, F.; Tu, B.; Yu, C.; Terasaki, O.; Zhao, D. *J. Am. Chem. Soc.* **2004**, *126*, 865.
(52) Jiao, F.; Harrison, A.; Jumas, J. C.; Chadwick, A. V.; Kockelmann, W.; Bruce, P. G. *J. Am. Chem. Soc.* **2006**, *128*, 5468.
(53) Boote, B.; Subramanian, H.; Ranjit, K. T. *Chem. Commun.* **2007**, 4543.

ordered 3D cubic $Ia\bar{3}d$ MCM-48 mesoporous silica. It is thus evident that such a structural transformation from 2D hexagonal *p6mm* to 3D cubic $Ia\bar{3}d$ requires a high stirring rate under low surfactant/silicon ratio (CTAB/TEOS = 0.16) compared to the original modified Stöber method with high surfactant/silicon ratio (CTAB/TEOS = 0.4).[47,48,53]

The phase formation of 2D hexagonal mesophase under diluted condition of surfactant with a low stirring rate can be explained as follows: First, the addition of more and more solvents of EtOH and H_2O will induce a diluting effect on the micelles making them less packed and smaller in size, which naturally favors a high surface curvature.[54] In addition, a large amount of EtOH will mostly act as a cosolvent in the mixture solution. This will slow the hydrolysis of TEOS and cause TEOS to be preferentially solvated into EtOH. The suppression of TEOS hydrolysis reduces the number of charged silicate moieties in the reaction solution, and subsequently increases the repulsive force between adjacent head groups of the surfactant. Therefore, the effective headgroup area (a_0) becomes larger, and it should be changed the surfactant packing parameter, g ($g = V/(a_0 l)$, where V is the total volume of the surfactant chain plus any cosolvent molecules between the chains, a_0 is the effective headgroup area at the organic−inorganic interface, and l is the surfactant chain length),[7,55] to decrease and favorably form 2D hexagonal mesophase instead of 3D cubic $Ia\bar{3}d$ mesophase.[56] However, at a high stirring rate under diluted surfactant conditions, TEOS hydrolysis can be more facilitated, which eventually could offset the factors for the formation of 2D hexagonal mesophase from cubic $Ia\bar{3}d$ mesophase described above. The synthetic recipe is currently the only available route to 3D cubic $Ia\bar{3}d$ mesoporous silica that allows kinetic control of phase transformation through the tuning of the stirring rate in the modified Stöber method.

The mesostructure of 3D cubic $Ia\bar{3}d$ symmetry can be readily obtained in a wide range of synthetic compositions by varying the combination of dilution of surfactant and amount of silica source at a high stirring rate. As shown in Figure 2, we can make a map for the 3D cubic $Ia\bar{3}d$ phase region by changing these two synthetic variables, simultaneously. For this phase diagram, all syntheses were performed at room temperature at a stirring rate of 850 rpm for 4 h. As can be seen, the region in which a well-developed cubic $Ia\bar{3}d$ phase is obtained is situated between a region of 2D hexagonal mesophase and a region of mixed phases. The poorly ordered mixed mesophase exhibiting several broad XRD diffraction peaks has been characterized as a mixed cubic-hexagonal phase (see Figure S2 in the Supporting Information).[57]

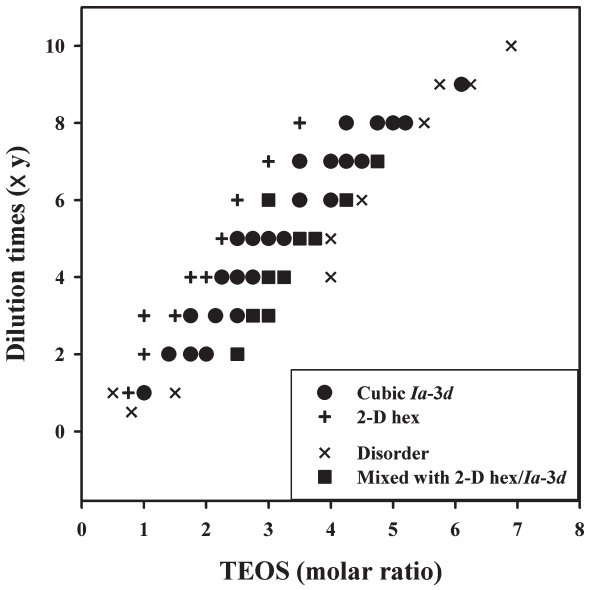

Figure 2. Phase diagram of mesophase structures established according to the XRD measurements. Each sample is prepared with a molar ratio of x:12.5y:54y:0.4:417y TEOS:NH_3:EtOH:CTAB:H_2O and stirring rate at 850 rpm for 4 h.

The phase region for the cubic $Ia\bar{3}d$ structure is reproducible, and it indicates an approximately linear relationship between the amounts of TEOS and the dilution times for CTAB surfactant. The synthesis interval ratios for the formation of the cubic $Ia\bar{3}d$ phase are CTAB/TEOS = 0.4/1.0−6.1 in molar ratio with 1−9 times diluted surfactant conditions. For the formation of cubic $Ia\bar{3}d$ mesophase under diluted CTAB concentration with a high stirring rate, the relationship between dilution times and TEOS amount is dilution time/TEOS molar ratio = 1.4−1.6. This indicates that in more diluted conditions and with a high stirring rate, a greater amount of silica source is required for the formation of cubic $Ia\bar{3}d$ mesostructure.

As shown in Figure 3, powder XRD patterns were measured on cubic $Ia\bar{3}d$ MCM-48 materials synthesized according to the initial compositions taken in the cubic phase domain, with a concurrent increase of the TEOS contents and dilution times for CTAB. All XRD diffraction patterns are able to index to cubic $Ia\bar{3}d$ mesophase. However, differences in the shape and position of XRD peaks and their relative intensities that correspond with changes in the TEOS amount and dilution times for CTAB. These differences in the XRD diffraction patterns indicate a variation of structural properties and sample quality. The shape and relative intensity of XRD peaks grew gradually sharper and increased up to 4 times dilution conditions, and then broadened and decreased, again. The nitrogen physisorption analyses provide more detailed structural properties. The resultant sorption isotherms, depicted in Figure S3 in the Supporting Information, are all type IV isotherms with a pronounced capillary condensation step around a relative pressure of P/P_0 = 0.2−0.3. The sharpness of the capillary condensation step is shown at 1−4 times diluted condition for CTAB surfactant, but higher diluted CTAB leads to less sharp capillary condensation, which indicates a lower

(54) Auvray, X.; Petipas, C.; Anthore, R.; Rico, I.; Lattes, A. *J. Phys. Chem.* **1989**, *93*, 7458.
(55) Huo, Q.; Margolese, D. I.; Stucky, G. D. *Chem. Mater.* **1996**, *8*, 1147.
(56) Liu, S. Q.; Cool, P.; Collart, O.; Van der Voort, P.; Vansant, E. F.; Lebedev, O. I.; Van Tendeloo, G.; Jiang, M. H. *J. Phys. Chem. B* **2003**, *107*, 10405.
(57) Tan, B.; Rankin, S. E. *J. Phys. Chem. B* **2004**, *108*, 20122.

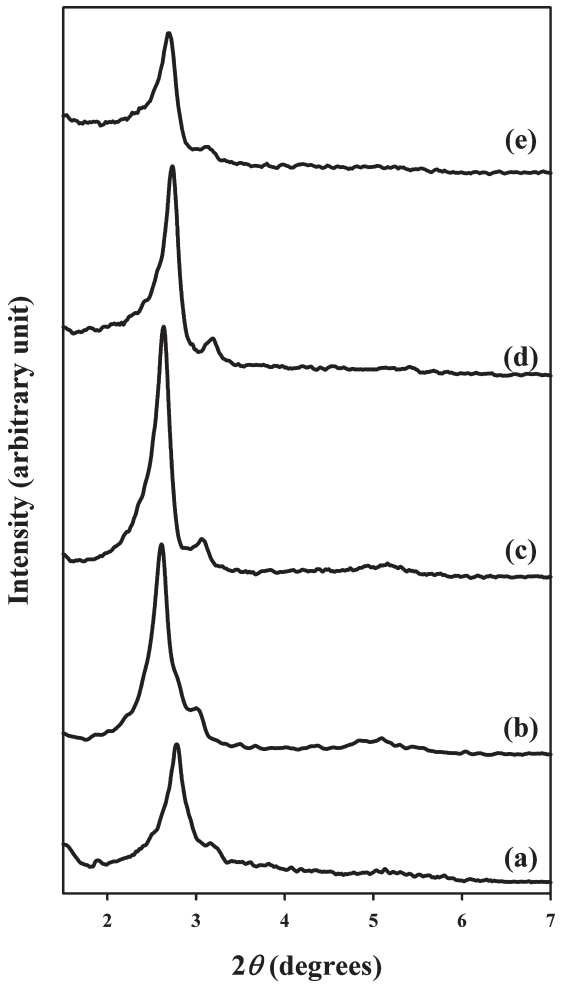

Figure 3. Powder XRD patterns for the calcined cubic $Ia\bar{3}d$ mesoporous MCM-48 silicas. Each sample was prepared as the molar ratio of x:12.5y:54y:0.4:417y TEOS:NH_3:EtOH:CTAB:H_2O, where x, y = (a) 1.0, 1 (b) 1.4, 2, (c) 2.5, 4, (d) 4.0, 6, and (e) 5.2, 8.

development of mesopores and low-quality mesoporous materials. The silica wall thickness is increased with the decrease of surfactant/TEOS molar ratio up to 4 times diluted condition (see Table S1 in the Supporting Information). The low surfactant/silicon ratio provides a several advantages compared to high surfactant/silicon ratio in terms of synthesizing the mesoporous silica materials: improvement of the stability of the entire mesostructure, increased framework thickness, and requirement of a smaller amount of surfactant.[58,59] In the present synthetic recipe, the thicker wall of 4 times diluted condition with low surfactant/silicon ratio could create a more stable mesostructure and prevent structural collapse during the calcination at high temperature.

Low-magnification SEM images (see Figure S4a−e in the Supporting Information) show the entire morphological aspect of each sample with different surfactant diluted conditions. At 4 times dilution (see Figure S4c,f in the Supporting Information), the whole feature of the SEM image is still aggregated single particles, but it forms smaller segments than in 1 and 2 times diluted conditions (see Figure S4a,b in the Supporting Information). A more diluted CTAB concentration leads to less particle aggregation. This indicates that lower surfactant concentration leads to less aggregation of particles. In addition, the individual particle size is around 300−600 nm (mostly ca. 500 nm), which is a more uniform particle size than when a high concentration of CTAB is used (150−600 nm, see Figure S1 in the Supporting Information). In Figure S4d, e,g in the Supporting Information, it can be seen that for more highly diluted CTAB conditions with lower surfactant/silicon ratio, the spherical particle size is similar to 4 times dilution, but an amorphous silica appears on the outside surface of the particle. This is wrapped with other spherical particles and creates a large aggregation. For the formation of cubic $Ia\bar{3}d$ mesophase, more diluted CTAB conditions with a high stirring rate require a greater amount of silica source per CTAB molar ratio. However, the amount of TEOS exceeds the amount of reacted CTAB when CTAB is highly diluted (more than 6 times dilution). The excess amount of TEOS results in amorphous silica and low-quality mesoporous materials. The SEM results for highly diluted conditions are coincident with the powder XRD, and the nitrogen physisorption results. From these results, well-developed 3D cubic $Ia\bar{3}d$ mesoporous silica nanoparticles with less aggregation are obtained when the syntheses are performed at 4 times diluted CTAB concentration with 2.5 TEOS molar ratio. This synthesis condition was employed to synthesize the materials as follows.

The stirring and aging times were varied between 30 s to 10 min and 0 min to 24 h, respectively, for a selected initial synthesis composition (4 times diluted condition: 2.5:50:216:0.4:1668 TEOS:NH_3:EtOH:CTAB:H_2O) to explore the optimum synthesis conditions for high-quality mesostructure and particle morphology. All samples were stirred at 1000 rpm using a digital mechanical stirrer (IKA Co.). The powder XRD patterns of the materials after filtration, washing, drying, and calcination at 823 K are reported in Figure 4. All silica samples synthesized through various stirring times and aging times exhibit diffraction patterns of the cubic $Ia\bar{3}d$ mesostructure. The results show that the MCM-48 mesostructure is built within a very short period of time (~30 s) under diluted CTAB conditions with a high stirring rate of 1000 rpm. The differences in XRD intensity and d-spacing reveal the stability and quality of the sample. The d-spacing of all samples is increased with longer time. In the stirring time experiment, the most noticeable increase occurs between 30 s and 1 min. (Figure 4a) After the addition of TEOS, facilitation of hydrolysis and condensation of the silica source with longer stirring results in a more stable and higher-quality cubic mesostructure in the initial synthetic mixture. However, a longer stirring time results in particle aggregation at extremely fast stirring speeds. In Figure 4b, the longer aging time leads to an increase in the d-spacing of samples after stopping mechanical stirring at 1 min. The XRD patterns of as-synthesized samples have almost the same d-spacing (data not shown), but the d-spacing was decreased more when aging time after

(58) Yu, J.; Shi, J.-L.; Wang, L.-Z.; Gao, J.-H.; Yan, D.-S. *J. Mater. Sci. Lett.* **2000**, *19*, 1461.
(59) Choma, J.; Pikus, S.; Jaroniec, M. *Appl. Surf. Sci.* **2005**, *252*, 562.

calcination was shortened. This indicates that a longer agitation time is required for further silica condensation, which in turn could prevent greater shrinkage of the mesostructure during calcination. The SEM images of samples with shorter stirring and agitation times are mostly similar to the samples synthesized at 850 rpm for 4 h (see Figure S4f in the Supporting Information). Most particles are fused together, even if variables of stirring and aging time are tuned. This shows that the particle morphology of MCM-48 at room temperature synthesis is determined at the initial synthesis time, and it is not so greatly dependent on dilution of surfactant, stirring rate, and aging time.

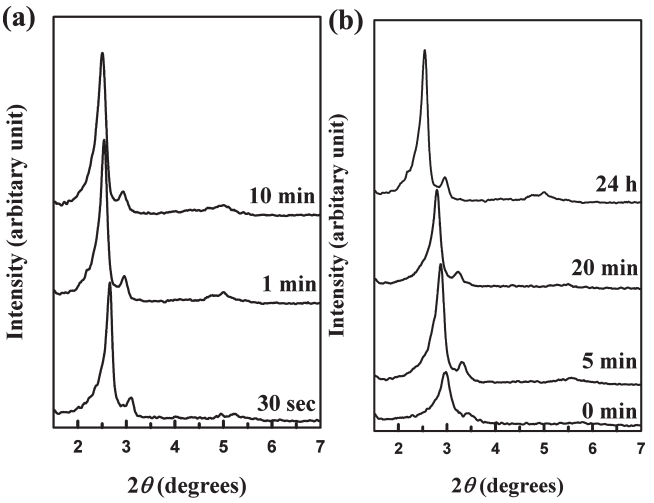

Figure 4. Powder XRD patterns for the calcined cubic $Ia\bar{3}d$ mesoporous MCM-48 silicas. Each sample was prepared as the molar ratio of 2.5:50:216:0.4:1668 TEOS:NH_3:EtOH:CTAB:H_2O. (a) Samples were obtained by different stirring time at 1000 rpm and aged 24 h, and (b) stirring for 1 min at 1000 rpm and different aging time.

3.2. Effect of F127 as a Dispersion Agent. For the synthesis of well size-defined and monodisperse MCM-48-type MSNs with controllable particle size below 500 nm, we studied the binary surfactant system using different nonionic surfactants (OP-10 (poly(ethylene glycol) monooctylphenyl ether)),[26] PEG-4000 (polyethylene glycol),[37] as well as triblock copolymer Pluronic F127,[29,31] and polymer (PVA (poly(vinyl) alcohol)[34] as particle grain-tailors. Maintaining the 4 times diluted CTAB concentration (2.5:50:216:0.4:1668 TEOS:NH_3:EtOH:CTAB:H_2O) at 1000 rpm for 1 min using mechanical stirrer, the morphology of MCM-48 MSNs with these inhibitors of grain growth still showed aggregated particle segments, with the exception of when Pluronic F127 was used. The addition of triblock copolymer Pluronic F127 as a nonionic surfactant decreased the size of the mesoporous silica particles produced by the assembly of the cationic surfactant and anionic silicate.[29,31] The effect of the amount of F127 on the particle morphology and size was investigated with TEM images. The TEM images in Figure 5b−d show that the well-dispersed spherical particle morphologies are obtained after the addition of a certain amount of F127, without aggregation between each

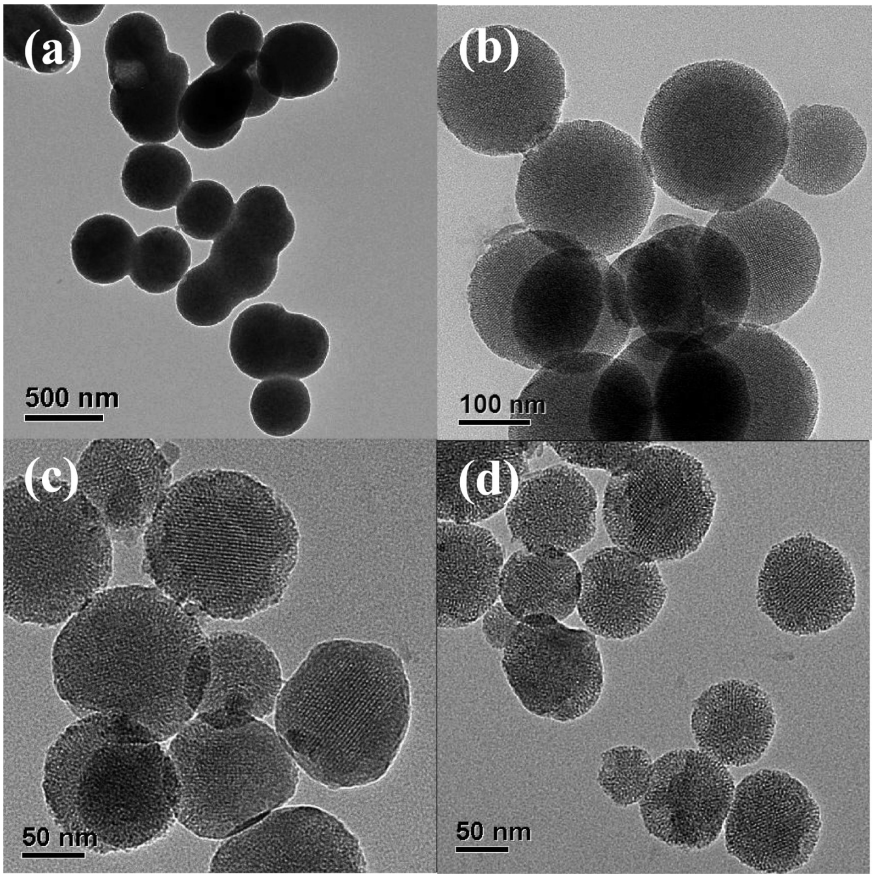

Figure 5. TEM images for calcined cubic $Ia\bar{3}d$ MCM-48 mesoporous silica nanoparticles with different amounts of the F127 under diluted CTAB concentration. F127 (in molar ratio) = (a) 0, (b) 0.047, (c) 0.078, and (d) 0.094.

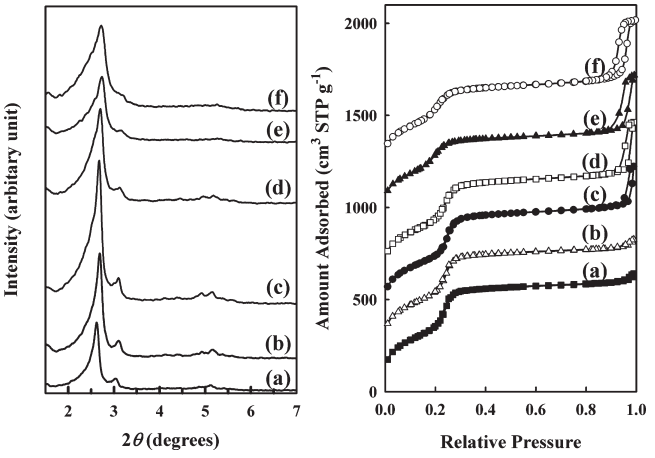

Figure 6. Powder XRD patterns (left) and nitrogen adsorption−desorption isotherm (right) for the calcined cubic $Ia\bar{3}d$ mesoporous MCM-48 silicas. Each sample was prepared as the molar ratio of 2.5:50:216:0.4:1668:x TEOS:NH_3:EtOH:CTAB:H_2O:F127, where x = (a) 0.016, (b) 0.031, (c) 0.047, (d) 0.063, (e) 0.078, and (f) 0.094. The isotherms for b−f samples are offset vertically by 200, 400, 600, 950, and 1200 cm^3 STP g^{-1}, respectively.

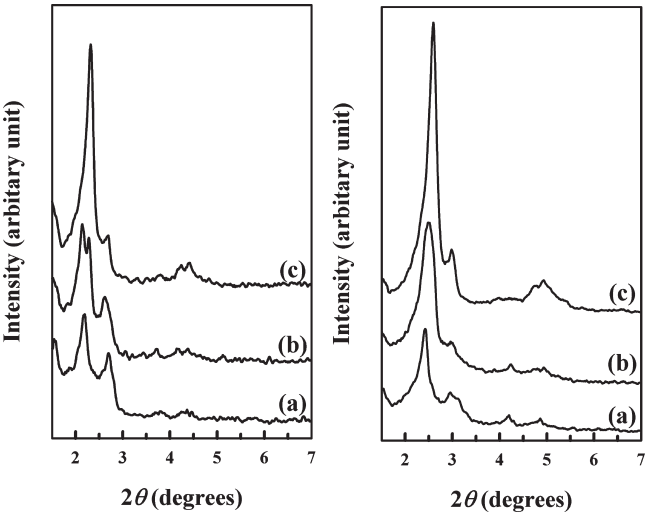

Figure 7. Powder XRD patterns for the as-synthesized (left) and calcined (right) cubic $Ia\bar{3}d$ mesoporous MCM-48 silicas using OTAB surfactant as a structure-directing agent. Each sample was prepared as the molar ratio of x:50:216:0.4:1668 TEOS:NH_3:EtOH:OTAB:H_2O, where x = (a) 2.5 (b) 2.0, and (c) 1.75.

particles. With an increase in amount of F127, the average particle size of separated grain is decreased from 500 to 70 nm. From the TEM images, it can be determined that the particle sizes range from 170 to 210 nm (size of most particles: ca. 200 nm), 80−180 nm (ca. 130 nm), and 40−100 nm (ca. 70 nm) for [F127] = 0.047, 0.078, and 0.094, respectively. Figure 6 shows powder XRD patterns and nitrogen physisorption isotherms for cubic $Ia\bar{3}d$ MCM-48 MSNs with different amounts of F127 molar ratio. All powder XRD patterns show the 3D cubic $Ia\bar{3}d$ mesophase, but the XRD diffraction peaks are broadened, with an increase in the F127 molar ratio above 0.047. This broadening of the diffraction peaks may cause a decrease in the reflection domains of mesophase from the decrease of spherical silica nanoparticle size.[31] The nitrogen isotherms provide more clear evidence for regarding the effect of the amount of F127. Each isotherm of MSN samples with different F127 amount exhibits two capillary condensation steps. The first step in a relative pressure range of 0.18−0.3 is attributed to the nitrogen condensation that took place at the internal mesopores, and the second step above 0.95 in the adsorption branch is due to interparticle voids, which indirectly reflects the size of particles: the higher step shows a small particle size. The size of the mesopores coming from CTAB for all samples is almost similar, at around 2.2−2.3 nm in diameter (see Table S2 in the Supporting Information), but the heights of both two capillary condensation steps are different, with an increase of the F127 amount. At a lower amount of F127, a sample shows the sharper step of the first capillary condensation, but smaller tailing in the second step. On the other hand, the higher amount of F127 gives a lower amount of N_2 adsorption in the first step but larger tailing in the second step. From these results, an increase in the amount of F127 results in highly monodisperse MCM-48-type MSN materials and a decrease of spherical particle size. We can obtain the monodisperse MCM-48-type MSN without the deformation of structural properties by using triblock copolymer F127 as a good dispersing agent and grain size tailor in the binary surfactant system. This indicates that the present synthesis method, diluted CTAB concentration with high stirring rate, could go through the route for cooperative assembly of silicate with the binary surfactant system.[29,31] The cationic surfactant, CTAB, is assembled with anionic silicates through electrostatic interaction in a basic solution, producing an ordered mesophase. The nonionic surfactant F127 interacted with silicates through the hydrogen bonds, limiting the growth of the mesostructure particle grain. Therefore, the grain size of the resultant mesoporous silica can be determined by the inhibition caused by the interaction with F127.

For the reproducible and scale-up test for the present synthesis recipe using diluted surfactant and low surfactant/silicon ratio with F127 as a particle size tailor, the synthesis was carried out in a larger batch using, for example, 4 g of CTAB in 1.2 L of F127-EtOH-NH_3-H_2O mixture solution. The powder XRD pattern, N_2 isotherm (see Figure S5 in the Supporting Information), and particle morphologies from TEM analysis of the large batch sample are similar to those of the small batch sample using 0.5 g of CTAB in 150 mL of mixture solution. This indicates that the production of monodisperse spherical MCM-48 MSN materials can be easily scaled up without any significant loss of sample quality due to the kinetically controlled short synthesis time.

3.3. Pore Size Control. *3.3.1. Synthesis of MCM-48 MSN Using OTAB.* To control the pore size of the MCM-48 MSNs, it is a well-known strategy to use different alkyl chain length cationic alkyltrimethylammonium surfactants via conventional hydrothermal synthesis route.[60] With the exception of CTAB, the successful synthesis of MCM-48 MSNs using other cationic alkytrimethylammoniumm surfactant via the Stöber method has never

(60) Kruk, M.; Jaroniec, M.; Ryoo, R.; Joo, S. H. *Chem. Mater.* **2000**, *12*, 1414.

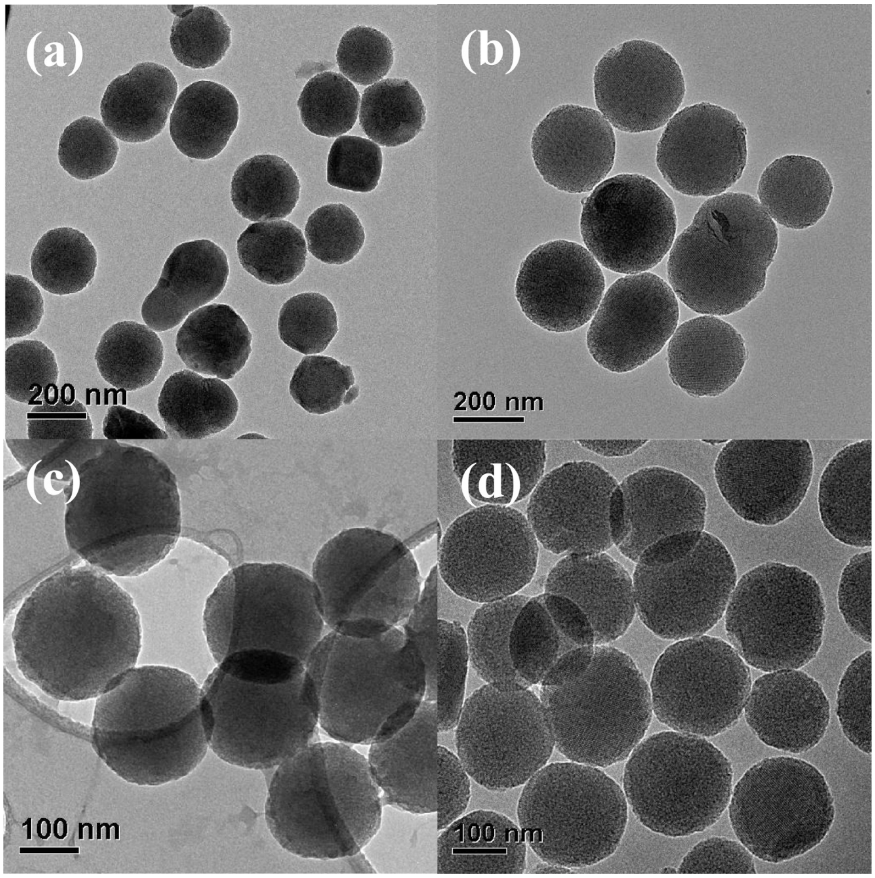

Figure 8. TEM images for the calcined cubic $Ia\bar{3}d$ mesoporous MCM-48 silicas using OTAB surfactant as a structure-directing agent. Each sample was prepared as the molar ratio of 1.75:50:216:0.4:1668:x TEOS:NH_3:EtOH:OTAB:H_2O:F127, where x = (a) 0, (b) 0.016, (c) 0.031, and (d) 0.047.

been reported before.[53,59] It should be noted that other different alkyl chain length surfactants were not suitable for MCM-48 synthesis at room temperature under the previous conditions of the modified Stöber method. Figure 7 shows the XRD patterns of as-synthesized and calcined mesoporous silica materials using octadecyltrimethylammonium bromide (OTAB), which has a longer alkyl chain length than CTAB. The samples were prepared with the present synthesis route as previously described: 4 times diluted surfactant concentration and mechanical stirring at 1000 rpm for 1 min, and then 1 day of aging at room temperature. At the same surfactant/silicon molar ratio for the optimum synthesis condition using CTAB surfactant (surfactant/TEOS = 0.4/2.5), the mesophase from OTAB surfactant shows hexagonal and cubic mix-phases. When the molar ratio of silica source was decreased from 2.5 to 1.75, the mesophase was clearly transformed from mix-phase and highly ordered 3D cubic $Ia\bar{3}d$ mesophase. This is the first successful synthesis of MCM-48 templated by alkylammonium surfactants other than cetyltrimethylammonium at room temperature synthesis. The phase transformation is the same trend that we discussed in the phase diagram for CTAB (Figure 2 and Figure S2 in the Supporting Information), but the amount of silica source is decreased for the synthesis of MCM-48 mesophase. The only difference from synthesis condition using CTAB is the surfactant chain length, and it should change the surfactant packing parameter, $g = V/(a_0 l)$. The longer chain length of OTAB has the direct influence on decreasing the value of g, which means that mesophase was transformed to MCM-41 ($1/3 < g < 1/2$) from MCM-48 ($1/2 < g < 2/3$). However, the phase transform goes through the a different way from cubic $Ia\bar{3}d$ to mixed hexagonal and cubic phase at the OTAB/TEOS = 0.4/2.5 molar ratio. This means the mesophase formation using the modified Stöber method under diluted surfactant condition with a high stirring rate is different from conventional hydrothermal synthesis. The mesophase formation can be kinetically controlled by the degree of TEOS hydrolysis and silicate polymerization, which is one of the important factor for structural transformation, by using the high stirring rate, and then the MCM-48 mesostructure is very quickly formed at around 30 s. (see Figure 1a,b) Further study on phase transformation of OTAB surfactant will be needed.

We also investigated the effect of F127 in OTAB surfactant as a dispersing agent and particle size tailor. MCM-48 mesoporous silica materials using OTAB were prepared at the molar ratio of 1.75:50:216:0.4:1668:0−0.047 TEOS:NH_3:EtOH:OTAB:H_2O:F127. As shown in Figure S6 in the Supporting Information, all XRD patterns are highly ordered cubic $Ia\bar{3}d$ mesostructures. Interestingly, both the d-spacing and the pore size were increased after the addition of F127. This suggests that a portion of F127 might be joined with OTAB surfactant during the assembly of the mesostructure, because OTAB

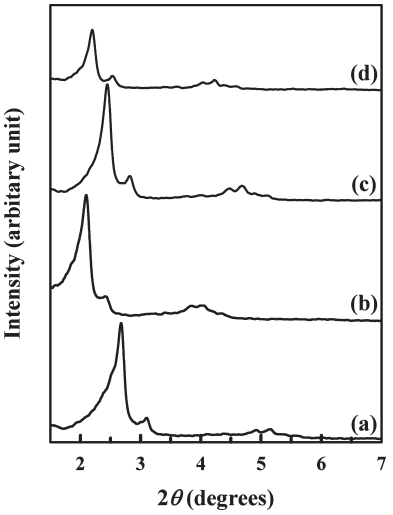

Figure 9. Powder XRD patterns for the calcined cubic $Ia\bar{3}d$ mesoporous MCM-48 silicas synthesized with different temperature. Samples (a) and (b) were prepared as the molar ratio of 2.5:50:216:0.4:1668:0.047 TEOS:NH_3:EtOH:CTAB:H_2O:F127, and (d) and (e) synthesized 1.75:50:216:0.4:1668:0.031 TEOS:NH_3:EtOH:OTAB:H_2O:F127. Samples (a) and (c) were synthesized at room temperature. Samples (b) and (d) were hydrothermally treated at 423 and 403 K for 2 days, respectively.

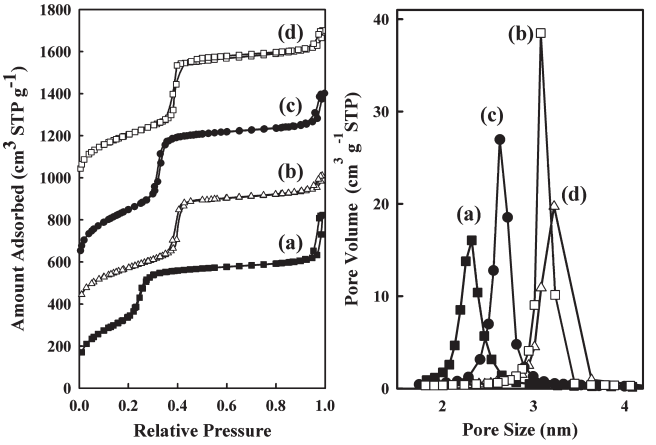

Figure 10. Nitrogen adsorption−desorption isotherm (left) and pore size distributions (right) for the calcined cubic $Ia\bar{3}d$ mesoporous MCM-48 mesoporous silicas synthesized at different temperatures. The isotherms for samples b−d are offset vertically by 300, 500, and 900 cm^3 STP g^{-1}, respectively. The pore size was analyzed with the adsorption branch using the BJH algorithm (see Figure 8 for sample composition).

Table 1. Structural Parameters of the 3D Cubic $Ia\bar{3}d$ MCM-48 MSNs Synthesized Using Different Alkyl Chain Length Surfactants and Post-Hydrothermal Treatment[a]

Sample	a (nm)	S_{BET} (m^2 g^{-1})	V_t (cm^3 g^{-1})	w_{BJH} (nm)	d (nm)
CTAB-RT	8.07	1248	0.96	2.3	1.45
CTAB-423 K	10.3	994	1.00	3.3	1.72
OTAB-RT	8.36	1258	1.03	2.4	1.50
OTAB-403 K	9.83	1116	1.11	3.1	1.64

[a] a, XRD unit cell parameter equals to $6^{1/2}d_{211}$; S_{BET}, apparent BET specific surface area deduced from the isotherm analysis in the relative pressure range from 0.05 to 0.20; V_t, total pore volume at relative pressure 0.95; w_{BJH}, the pore diameter calculated using the BJH method. d, wall thickness evaluated by $d = a/3.092 - w_{BJH}/2$.[48] The sample notations of CTAB-RT and CTAB-423 K mean MSNs are synthesized using CTAB at room temperature and CTAB with post-hydrothermal treatment at 423 K for 2 days, respectively. (see Figure 9 for the synthesis molar ratios).

surfactant might have more hydrophobicity than CTAB. But the reason for the joining of F127 and OTAB is still unclear, and also demands further investigation. The nitrogen isotherm of the sample without F127 also shows a distinct capillary condensation step in the range of $P/P_0 > 0.95$ (see Figure S6 in the Supporting Information). The structural properties of the samples synthesized from OTAB surfactant have almost the same values, but pore size of the sample was increased from 2.4 to 2.6 nm after addition of F127 (see Table S3 in the Supporting Information), like d-spacing from XRD patterns. From the TEM analysis in Figure 8, it was determined that the synthesis condition using OTAB template without F127 gives more monodisperse MSNs than the synthesis condition using CTAB without F127. In the synthesis condition using OTAB, the relatively lower amount of silica source might make to reduce the chance for single particles to fuse together, and then gives more monodisperse MCM-48 MSN. The particle size of MSN with no F127 is 200−230 nm in diameter but a part of particle morphology shows aggregation between two single particles. With an increase of the amount of F127, the number of aggregated morphologies is decreased and finally monodispersed single particles are shown at F127 molar ratio above 0.031. In addition, the range of particle sizes was also gradually decreased from 200 to 230 nm to 160−200 nm when the amount F127 was increased from 0.016 to 0.047 molar ratio. Like the synthesis using CTAB surfactant, it will be possible to obtain much smaller nanoparticles using additional F127.

3.3.2. Posthydrothermal Treatment. For the more precise tailoring of the textural parameters of the cubic $Ia\bar{3}d$ MCM-48 mesoporous silica nanoparticles, posthydrothermal treatment at 403 and 423 K for 2 days was applied to selected compositions (2.5:50:216:0.4:1668:0.047 TEOS:NH_3:EtOH:CTAB:H_2O:F127 and 1.75:50:216:0.4:1668:0.031 TEOS:NH_3:EtOH:OTAB:H_2O:F127). The XRD patterns of the calcined materials are reported in Figure 9. The MSNs synthesized with hydrothermal treatment all exhibit highly resolved diffraction patterns characteristic of the cubic $Ia\bar{3}d$ mesostructure. A noticeable increase in the d-spacing, and hence the lattice parameters, occurs when an increased temperature is applied for the additional hydrothermal treatment compared to room temperature synthesis. Figure 10 shows the nitrogen sorption isotherms and pore size distributions for the same series of samples. The sorption isotherms for the different calcined samples remain type IV isotherms with a sharp capillary condensation step after hydrothermal treatment. The shift of the capillary condensation step to a higher relative pressure with increasing temperature evidence an increase in the mesopore size, which was also indicated by the pore size distribution curves. Structural and textural properties for these samples are summarized in Table 1. The pore volumes are shown to increase slightly, and the pore sizes range from 2.3 to 3.3 nm for

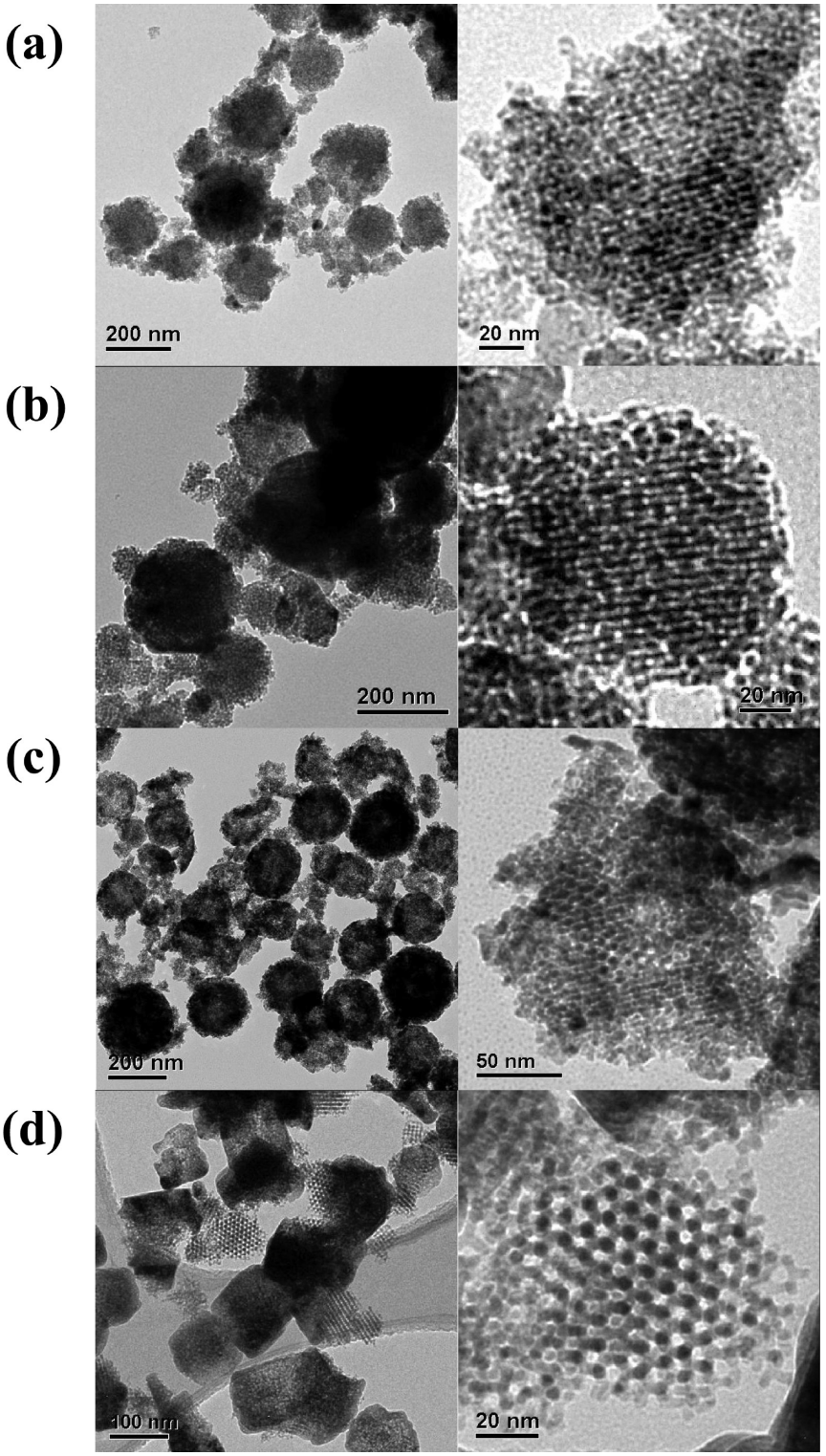

Figure 11. TEM images and the high magnified TEM images (right) for mesoporous metal oxide replicas prepared using MCM-48 silica nanoparticles: (a) Fe_2O_3 (b) Co_3O_4 (c) CeO_2 and (d) In_2O_3.

this series of samples. The lattice parameter of the cubic mesophase increases from 8.07 nm at room temperature up to 10.3 nm for the mesoporous materials prepared at 423 K using CTAB surfactant. Moreover, the wall thickness is shown to increase with increasing posthydrothermal temperature. It has to be noted that a rearrangement of the silica framework has taken place at the high temperature during the hydrothermal treatment.[50] The morphology of MSNs still remains as separated spherical silica nanoparticles after posthydrothermal treatment, but some portion of the MSN particles adhere to other particles (see Figure S7 in the Supporting Information).

3.4. Mesoporous Metal Oxide Nanoparticles. Various kinds of mesoporous metal oxide nanoparticles were successfully synthesized using MCM-48-type MSNs as a

mold via a template synthesis route.[61] The synthesis of various mesoporous metal oxides was simply prepared by repeated impregnation with the desired metal precursors, and a calcination process.[51,52] As shown in Figure S8 in the Supporting Information, the XRD patterns of the mesoporous metal oxide nanoparticles, iron oxide (Fe_2O_3), cobalt oxide (Co_3O_4), cerium oxide (CeO_2), and indium oxide (In_2O_3), show a single weak diffraction peak in the region of the low angle, which can be indexed to (211) reflection by the determination of the peak position. Each of the mesoporous metal oxides can be determined by the reflection peaks in the region of the wide angle. After removal of the silica template, structurally transformed mesoporous structures could be produced using MCM-48 templates, which is a well-known phenomenon in the case of ordered mesoporous carbon CMK-1.[39,42,61] This structure transformation can be determined from the appearance of the additional (110) reflection peak below the 2θ value of (211) reflection. However, we cannot distinguish any additional XRD peaks because of the low intensity and high background noise of XRD diffraction. This indicates that these mesoporous metal oxide nanoparticles have small particle morphologies, or less ordering and structural deficiency, which are typically caused by the transformation from metal oxide precursors to metal oxides during the calcination.[62] All metal oxides exhibit type IV isotherm shape with hysteresis loop and 4.8−6.3 nm of pore size. These larger pore diameters with broad pore size distribution compared to ordered mesoporous carbon CMK-1 (ca. 2.3 nm in a diameter) might also be caused by large lattice contractions during the thermal treatment and less ordered mesostructures.[62] As shown in Table S4 in the Supporting Information, the BET areas and pore volumes of mesoporous metal oxide nanoparticles are 139−213 m^2/g and 0.15−0.32 cm^3/g, except for In_2O_3. The mesoporous Indium oxide nanoparticle has relatively small values of BET area (49 m^2/g) and pore volume (0.09 cm^3/g) compared to other metal oxides. As shown in Figure 11, the TEM images clearly show the morphology of mesoporous metal oxide nanoparticles as well as their mesostructural pore-ordering. The highly magnified TEM images show that all mesoporous metal oxide nanoparticles have a well-ordered mesopore arrangement. The morphologies of all mesoporous metal oxides, except for In_2O_3, reveal mostly spherical nanoparticles, which is the same as an MCM-48 MSN template. This indicates that the morphology of MSN is well-preserved in the mesoporous metal oxides during the replication process. But it also shows small irregular particles, which are believed to be caused by the incompletely filling of metal oxide precursors into the pores of MSN template. The rectangular particle shape and the partially rectangular shape with highly ordered mesopore structures are shown in the case of In_2O_3. From the low surface area and pore volume of mesoporous indium oxide nanoparticle in N_2 physisorption analysis, we could deduce that this rectangular morphology is a growth of bulk indium oxide with a cubic crystalline morphology, which is located outside the surface of the MSN template and covered with spherical mesoporous metal oxides. The high crystallinity of In_2O_3 in wide-angle XRD pattern also confirms the existence of the outside deposition of indium oxide (see Figure S8 in the Supporting Information). This could be overcome to find an optimum amount of indium oxide precursor through a repeated impregnation-calcination process.

4. Conclusions

The preparation method for monodisperse spherical MCM-48 mesoporous nanoparticles with a 3D cubic $Ia\bar{3}d$ mesostructure, which is based on the use of a modified Stöber method, is easy and highly reproducible. The synthesis is simply carried out by the mechanical stirring of the basic surfactant template solution at 1000 rpm for 1 min at room temperature, after the addition of silica source. This method, kinetically controlled phase transformation by high stirring rate under low surfactant/silicon ratio, has made it possible to synthesize cubic $Ia\bar{3}d$ mesophase in a wide range of mixture compositions, and gives synthetic phase diagram in the function of surfactant concentration and amount of silicon source. Most importantly, monodisperse spherical MCM-48 MSN was easily achieved with precise control of the particle size by using triblock copolymer Pluronic F127 as a dispersing agent. Moreover, the pore diameter of MCM-48 MSNs could be tuned using different alkyl chain surfactants, and through simple posthydrothermal treatment. The MCM-48-type MSNs with tailored structural properties thus obtained can be used as a versatile hard template for the preparation of new nonsiliceous mesoporous nanoparticles such as metal, metal oxides, carbons, and polymers. Furthermore, 3D enantiomeric pairs of porous channel mesoporous structures with utrafine nanoparticles are particularly suitable as materials for the application of adsorption, delivery and release, and host−guests interactions.

Acknowledgment. This study was supported by the U.S. DOE Ames Laboratory through the office of Basic Energy Sciences under Contract DE-AC02-07CH11358.

Supporting Information Available: SEM images of the calcined mesoporous silica materials obtained using magnetic stirrer with different stirring rate; powder XRD patterns for the calcined mesoporous silica materials obtained under 4 times diluted condition using magnetic stirrer at 850 rpm for 4 h with different TEOS molar ratio; nitrogen adsorption−desorption isotherm for the mesostructured silica materials obtained using x:12.5y:54y:0.4:417y TEOS:NH_3:EtOH:CTAB:H_2O; SEM images of the calcined mesoporous silica materials obtained using magnetic x:12.5y:54y:0.4:417yx TEOS:NH_3:EtOH:CTAB:H_2O; powder XRD patterns and

(61) Kim, T.-W.; Chung, P.-W.; Slowing, I. I.; Tsunoda, M.; Yeung, E. S.; Lin, V. S. Y. *Nano Lett*. **2008**, *8*, 3724.
(62) Kang, M.; Kim, D.; Yi, S. H.; Han, J. U.; Yie, J. E.; Kim, J. M. *Catal. Today* **2004**, *93−95*, 695.

nitrogen adsorption−desorption isotherm for the calcined large batch cubic $Ia\bar{3}d$ mesoporous MCM-48 silica after posthydrothermal treatment at 423 K for 2 days; powder XRD patterns and nitrogen adsorption−desorption isotherm for the calcined cubic $Ia\bar{3}d$ mesoporous MCM-48 silicas with the molar ratio of 1.75:50:216:0.4:1668:x TEOS:NH_3:EtOH:OTAB:H_2O:F127. TEM images for the calcined cubic $Ia\bar{3}d$ mesoporous MCM-48 MSN after posthydrothermal treatment at 423 K for 2 days; low-angle and wide-angle XRD patterns for the mesoporous metal oxide materials; nitrogen adsorption−desorption isotherm and corresponding pore size distributions for the mesoporous metal oxide materials (PDF). This material is available free of charge via the Internet at http://pubs.acs.org.